

# Efficiency of the centrifugally induced curvature drift instability in AGN winds.

Osmanov Z.

E. Kharadze Georgian National Astrophysical Observatory, Kazbegi str. 2a, 0106 Tbilisi  
e-mail: z.osmanov@astro-ge.org

Preprint online version: February 10, 2022

## ABSTRACT

*Aims.* For studying how the field lines are twisting nearby the light cylinder surface, which provides the free motion of AGN winds through the mentioned area, the investigation of the centrifugally driven curvature drift instability is presented.

*Methods.* Studying the dynamics of the relativistic MHD flow close to the light cylinder surface, by applying a single particle approach based on the centrifugal acceleration, the dispersion relation of the instability is derived and analytically solved.

*Results.* Considering the typical values of AGN winds, it is shown that the time scale of the curvature drift instability is much less than the accretion process time scale, indicating that the present instability is very efficient and might strongly influence processes in AGN plasmas.

**Key words.** active galaxies – instabilities – acceleration of particles – magnetohydrodynamics – plasma physics

## 1. Introduction

For studying the AGN winds the fundamental problem relates to the understanding of a question: how the plasma goes through the Light Cylinder Surface (LCS - the hypothetical zone, where the linear velocity of rotation equals the speed of light). An innermost region of AGNs is characterized by the rotational motion, and it is obvious that such a character of motion must affect the plasma dynamics. According to the standard model, the magnetic field due to the frozen-in condition undergoes plasmas and consequently the flow follows the field lines, co-rotating with them. This means that the plasma particles moving along quasi straight magnetic field lines in the nearby area of the LCS have to reach the speed of light. On the other hand no physical system can maintain such a motion and this fact must result in a certain twisting process of the magnetic field lines on the LCS. Generalizing the work: (Machabeli & Rogava 1994) for curved trajectories, by Rogava et al. (2003) the dynamics of a single particle moving along a prescribed rotating curved channel has been investigated. It was shown that if the trajectories are given by the Archimedes spiral, the particles can cross the LCS avoiding the light cylinder problem. Making one more step to this investigation is to find an appropriate mechanism, which might provide the twisting of the magnetic field lines, giving rise to the shape of the Archimedes spiral, which in turn makes the dynamics force-free.

The light cylinder problem in the context of the force-free regime has been extensively studied numerically for pulsars. The investigation developed in (Spitkovsky & Arons 2002, Spitkovsky 2004) has shown that the plasmas can go through the LCS. This work was based on a current generated by the electric drift (Blandford 2002), which is vanishing for quasi neutral plasmas and can not give a contribution in the dynamics of astrophysical flows having almost equal numbers of positive and negative charges.

Since the innermost region of AGNs is rotating, a role of the Centrifugal Force (CF) seems to be particularly interesting for the study of the relativistic plasma motion. The centrifugally driven outflows have been discussed in series of works. A special attention deserves the work of Blandford & Payne (1982), where the authors discuss the possibility of the energy and angular momentum pumping from the accretion disk, emphasizing the role of the centrifugal acceleration in this process. By Gangadhara & Lesch 1997 the CF was considered in the context of the non thermal radiation from the spinning AGNs. Generalizing the mentioned work it has been shown (Osmanov et al. 2007, Rieger & Aharonian 2008) that due to the centrifugal acceleration, electrons gain very high energies with Lorentz factors up to  $\gamma \sim 10^8$ . This means that the energy budget in the AGN winds is very high and if one finds a mechanism of the conversion of at least a small fraction of this energy into a variety instabilities, one might have interesting consequences in the physics of AGN outflows.

The centrifugal force may drive different kinds of instabilities. Obviously the CF acting on a moving particle changes in time and in the context of instabilities plays a role of the parameter. Consequently the corresponding instability is called the parametric instability.

The centrifugally driven parametric instability first has been introduced in (Machabeli et al. 2005) for the Crab pulsar magnetosphere. We have argued that the centrifugal force may cause the separation of charges, leading to the creation of an unstable electrostatic field. Estimating the linear growth rate it has been shown that the instability was extremely efficient. The method developed in (Machabeli et al. 2005) was applied for AGN jets (Osmanov 2008) for studying the stability problem of the rotation induced electrostatic instability and for understanding how efficient is the centrifugal acceleration in this process. Another kind of the instability which might be induced by the CF is the so called Curvature Drift Instability (CDI). Even if the field lines initially have a very small curvature, it might

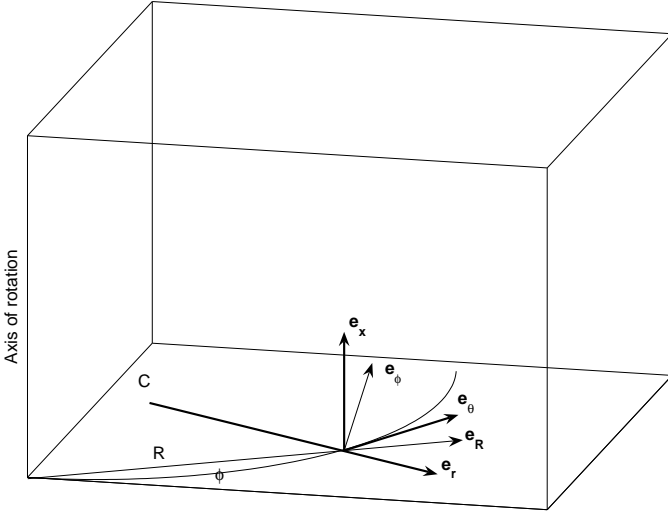


**Fig. 1.** Two orthonormal bases are considered: i) cylindrical components of unit vectors, ( $\mathbf{e}_\phi$ ,  $\mathbf{e}_R$ ,  $\mathbf{e}_x$ ); ii) unit vectors of the system rigidly fixed on each point of the curve, ( $\mathbf{e}_r$ ,  $\mathbf{e}_\theta$ ,  $\mathbf{e}_x$ ), respectively.  $C$  is the center of the curvature. Hereafter the set of coordinates I call the field line coordinates.

cause a drifting process of plasmas, leading to the CDI. By Osmanov et al. (2008a) the two component relativistic plasma has been considered for studying the role of the centrifugal acceleration in the curvature drift instability for pulsar magnetospheres. The investigation has shown that the growth rate was more than pulsar spin down rates by many orders of magnitude, indicating high efficiency of the CDI. The curvature drift current produces the toroidal component of the magnetic field, which due to the efficient unstable character of the process amplifies rapidly, changing the overall configuration of the magnetic field. This leads to the transformation of field lines into the shape of the Archimedes spiral, when the motion of the particles switches to the so called force-free regime (Osmanov et al. 2008b) and the plasma goes through the LCS.

In the present paper in order to investigate the twisting process of magnetic field lines due to the CDI, the method developed in (Osmanov et al. 2008a, Osmanov et al. 2008b) will be implemented for AGN winds.

The paper is arranged as follows. In §2 we introduce the curvature drift waves and derive the dispersion relation. In §3 the results for typical AGNs are present and in §4 we summarize our results.

## 2. Main consideration

We start the investigation by considering the two component plasma consisting of the relativistic electrons with the Lorentz factor  $\gamma_e \sim 10^{5-8}$  (Osmanov et al. 2007, Rieger & Aharonian 2008) and the bulk component (protons) with  $\gamma_b \sim 10$ . Since we are interested in the twisting process, we suppose that initially the field lines are almost rectilinear in order to study how this configuration changes in time.

Let us start by the Euler equation governing the dynamics of plasma particles, co-rotating with the straight magnetic field lines. By applying the method developed by Chedia et al. (1996) one can show that the Euler equation gets the following form:

$$\frac{\partial \mathbf{p}_\alpha}{\partial t} + (\mathbf{v}_\alpha \nabla) \mathbf{p}_\alpha = -\gamma_\alpha \xi \nabla \xi + \frac{q_\alpha}{m_\alpha} (\mathbf{E} + \mathbf{v}_\alpha \times \mathbf{B}), \quad (1)$$

$$\alpha = \{e, b\},$$

where

$$\xi \equiv \sqrt{1 - \Omega^2 R^2 / c^2}.$$

Here  $\mathbf{p}_\alpha$  is the momentum,  $\mathbf{v}_\alpha$  - the velocity and  $\gamma_\alpha$  - the Lorentz factor of the relativistic particles.  $\mathbf{E}$  and  $\mathbf{B}$  are the electric field and the magnetic induction respectively. By  $q_\alpha$  and  $m_\alpha$  we denote particle's charge and the rest mass respectively. We express the equation of motion in the cylindrical coordinates (see Fig. 1). The first term of the right hand side of the Euler equation  $-\gamma_\alpha \xi \nabla \xi$  represents the centrifugal force, which on the light cylinder surface becomes infinity. This means that its overall effect is significant in the nearby zone of the LCS. For describing our physical system, one needs the full set of equations, and in order to close the system, we add to Eq. (1) the continuity equation:

$$\frac{\partial n_\alpha}{\partial t} + \nabla(n_\alpha \mathbf{v}_\alpha) = 0, \quad (2)$$

and the induction equation:

$$\nabla \times \mathbf{B} = \frac{1}{c} \frac{\partial \mathbf{E}}{\partial t} + \frac{4\pi}{c} \sum_{\alpha=e,b} \mathbf{J}_\alpha, \quad (3)$$

where  $n_\alpha$  and  $\mathbf{J}_\alpha$  are the density and the current, respectively.

In the zeroth approximation the plasma particles undergo only the centrifugal force. Different species at different positions experience different CFs, which will cause the separation of charges, leading to the creation of the additional electromagnetic field considered as the first order term in our equations.

The leading state is characterized by the frozen-in condition,  $\mathbf{E} + \mathbf{v}_\alpha \times \mathbf{B}_0 = \mathbf{0}$ , which reduces Eq. (1) into the following form (Machabeli & Rogava 1994):

$$\frac{dv}{dt} = \frac{\Omega^2 R}{1 - \frac{\Omega^2 R^2}{c^2}} \left[ 1 - \frac{\Omega^2 R^2}{c^2} - \frac{2v^2}{c^2} \right]. \quad (4)$$

The present equation of motion describing the kinematic behaviour of the single co-rotating particle has the following solution:

$$v(t) \equiv v_\parallel \approx c \cos(\Omega t), \quad (5)$$

for ultra relativistic cases ( $\gamma \gg 1$ ) and the following initial conditions:  $R(0) = 0$ ,  $v(0) \approx c$  ( $v \equiv dR/dt$ ). Here  $v_\parallel$  denotes the velocity component along the magnetic field lines.

Since we suppose that the magnetic field lines initially have the small curvature, the particles moving radially, will drift along the  $x$  axis as well (Osmanov et al. 2008a) (see Fig. 1). The mentioned drift of charges will produce the corresponding current, which inevitably will create the toroidal magnetic field, changing the overall configuration of the field lines. Therefore the aim of the present work is to study the role of the centrifugally induced curvature drift instability in the twisting process of the magnetic field lines. For this purpose one can linearize the system of equations Eqs. (1-3), perturbing all physical quantities around the leading state:

$$\Psi \approx \Psi^0 + \Psi^1, \quad (6)$$

$$\Psi = \{n, \mathbf{v}, \mathbf{p}, \mathbf{E}, \mathbf{B}\}. \quad (7)$$

Let us express the perturbation by following:

$$\Psi^1(t, \mathbf{r}) \propto \Psi^1(t) \exp[i(\mathbf{k}\mathbf{r})], \quad (8)$$

then from Eqs. (1-3) one can derive the linearized set of equations governing the CDI:

$$\frac{\partial p_{\alpha x}^1}{\partial t} - i(k_x u_\alpha + k_\phi v_\parallel) p_{\alpha x}^1 = \frac{q_\alpha}{m_\alpha} v_\parallel B_r^1, \quad (9)$$

$$\frac{\partial n_\alpha^1}{\partial t} - i(k_x u_\alpha + k_\phi v_\parallel) n_\alpha^1 = i k_x n_\alpha^0 v_{\alpha x}^1, \quad (10)$$

$$-i k_\phi c B_r^1 = 4\pi \sum_{\alpha=e,b} q_\alpha (n_\alpha^0 v_{\alpha x}^1 + n_\alpha^1 u_\alpha). \quad (11)$$

Here by  $u_\alpha$  we denote the curvature drift velocity along the  $x$  axis:

$$u_\alpha = \frac{\gamma_{\alpha 0} v_\parallel^2}{\omega_B R_B}, \quad (12)$$

where  $\omega_{\alpha B} = q_\alpha B_0 / m_\alpha c$ ;  $R_B$  is the curvature radius of magnetic field lines; and

$$B_0 = \sqrt{\frac{2L}{R_{lc} c^2}} \quad (13)$$

is the equipartition magnetic induction on the LCS for the leading state (here  $L$  is the luminosity of the AGN and  $R_{lc} = c/\Omega$  is the light cylinder radius). For deriving Eqs. (9-11) the wave propagating almost perpendicular to the equatorial plane has been considered and the expression:  $v_r^1 \approx c E_x^1 / B_0$  was taken into account. For simplicity the set of equations are given in the coordinates of the field line (see Fig. 1).

Let us express  $v_{\alpha x}^1$  and  $n_\alpha^1$  by the following way:

$$v_{\alpha x}^1 \equiv V_{\alpha x} e^{i\mathbf{k}\mathbf{A}_\alpha(t)}, \quad (14)$$

$$n_\alpha^1 \equiv N_\alpha e^{i\mathbf{k}\mathbf{A}_\alpha(t)}, \quad (15)$$

where

$$A_{\alpha x}(t) = \frac{u_\alpha t}{2} + \frac{u_\alpha}{4\Omega} \sin(2\Omega t), \quad (16)$$

$$A_{\alpha\phi}(t) = \frac{c}{\Omega} \sin(\Omega t). \quad (17)$$

Then, by substituting Eqs. (14,15) into Eqs. (9-11), it is easy to solve the system for the toroidal component:

$$\begin{aligned} -i k_\phi c B_r^1(t) &= \sum_{\alpha=e,b} \frac{\omega_\alpha^2}{\gamma_{\alpha 0}} e^{i\mathbf{k}\mathbf{A}_\alpha(t)} \int e^{-i\mathbf{k}\mathbf{A}_\alpha(t')} v_\parallel(t') B_r(t') dt' + \\ &i \sum_{\alpha=e,b} \frac{\omega_\alpha^2}{\gamma_{\alpha 0}} k_x u_\alpha e^{i\mathbf{k}\mathbf{A}_\alpha(t)} \int dt' \int e^{-i\mathbf{k}\mathbf{A}_\alpha(t'')} v_\parallel(t'') B_r(t'') dt'' \end{aligned} \quad (18)$$

where  $\omega_\alpha = e \sqrt{4\pi n_\alpha^0 / m_\alpha}$  is the plasma frequency. After making the Fourier transform (see Appendix A), Eq. (18) gets the form:

$$B_r(\omega) = - \sum_{\alpha=e,b} \frac{\omega_\alpha^2}{2\gamma_{\alpha 0} k_\phi c} \sum_{\sigma=\pm 1} \sum_{s,n,l,p} \frac{J_s(g_\alpha) J_n(h) J_l(g_\alpha) J_p(h)}{\omega + \frac{k_x u_\alpha}{2} + \Omega(2s+n)} \times$$

$$\begin{aligned} &\times B_r(\omega + \Omega(2[s-l] + n - p + \sigma)) \left[ 1 - \frac{k_x u_\alpha}{\omega + \frac{k_x u_\alpha}{2} + \Omega(2s+n)} \right] \\ &+ \sum_{\alpha=e,b} \frac{\omega_\alpha^2 k_x u_\alpha}{4\gamma_{\alpha 0} k_\phi c} \sum_{\sigma,\mu=\pm 1} \sum_{s,n,l,p} \frac{J_s(g_\alpha) J_n(h) J_l(g_\alpha) J_p(h)}{\left(\omega + \frac{k_x u_\alpha}{2} + \Omega(2[s+\mu] + n)\right)^2} \times \\ &\times B_r(\omega + \Omega(2[s-l+\mu] + n - p + \sigma)), \end{aligned} \quad (19)$$

where

$$g_\alpha = \frac{k_x u_\alpha}{4\Omega}, \quad h = \frac{k_\phi c}{\Omega}.$$

Let us note that Eq. (19) is written for  $B_r(\omega)$  and on the right hand side of the equation, there is the infinite number of components with  $B_r(\omega \pm \Omega)$ ,  $B_r(\omega \pm 2\Omega)$ ,... etc. This means that for solving the mentioned equation, thus for closing the system, one needs to add the corresponding expressions for  $B_r(\omega \pm \Omega)$ ,  $B_r(\omega \pm 2\Omega)$ ,... etc. But then the system becomes composed of the infinite number of equations, making the task unsolvable. In order to overcome this problem one has to use a certain, physically reasonable cutoff on the right hand side of the equation (Silin et al. 1970). As it is clear from Eq. (19), the considered instability is characterized by the following proper frequency of the curvature drift modes:

$$\omega_0 \approx -\frac{k_x u_\alpha}{2}, \quad (20)$$

when the corresponding conditions:  $k_x u_\alpha / 2 < 0$ ,  $2s + n = 0$  and  $2[s + \mu] + n = 0$  are satisfied. As we will see only the resonance terms give the significant contribution to the result.

Let us consider parameters  $L \sim 10^{44} \text{ erg/s}$ ,  $\Omega = 3 \times 10^{-5} \text{ s}^{-1}$ ,  $\gamma_{e0} \sim 10^5$ ,  $R_B \approx R_{lc}$ ,  $n_{e0} \sim 0.001 \text{ cm}^{-3}$  typical for AGN winds. Then examining the curvature drift waves with  $\lambda \sim R_{lc}$  ( $\lambda = 2\pi/k$  is the wave length), one can show that  $|k_x u_e / 2| \sim 10^{-12} \text{ s}^{-1} \ll \Omega$  (here, it is supposed that  $k_x < 0$  and  $u_{e0} > 0$ , otherwise the frequency becomes negative). Therefore all terms with non zero  $\Omega(2s+n)$  and  $\Omega(2[s+\mu]+n)$  are rapidly oscillative and do not contribute in the final result. Consequently the only terms, which influence the solution of Eq. (19) are the leading terms, the contribution of which reduces the equation (Osmanov et al. 2008a) (see Appendix B):

$$\left(\omega + \frac{k_x u_e}{2}\right)^2 \approx \sum_{\sigma,\mu=\pm 1} \sum_{s,l} \Xi_\mu J_s(g) J_{n'(s,\mu)}(h) J_l(g) J_{p'(l,\sigma)}(h), \quad (21)$$

where

$$\begin{aligned} \Xi_0 &= 2\Xi_{\pm 1} = \frac{\omega_e^2 k_x u_e}{2\gamma_{ep0} k_\phi c}, \\ n' &= -2(s + \mu), \quad p' = -2l + \sigma, \quad g \equiv g_e. \end{aligned} \quad (22)$$

Note, that Eq. (21) does not consist of the bulk components at all, because as a direct calculation shows, their contribution is negligible with respect to the terms corresponding to the relativistic electrons. Expressing the frequency by the real and imaginary parts:  $\omega \equiv \omega_0 + i\Gamma$  it is straightforward to show from Eq. (21), that the increment of the CDI writes as :

$$\Gamma \approx \left[ \sum_{\sigma,\mu=\pm 1} \sum_{s,l} \Xi_\mu J_s(g) J_{-2(s+\mu)}(h) J_l(g) J_{-2l+\sigma}(h) \right]^{\frac{1}{2}}. \quad (23)$$

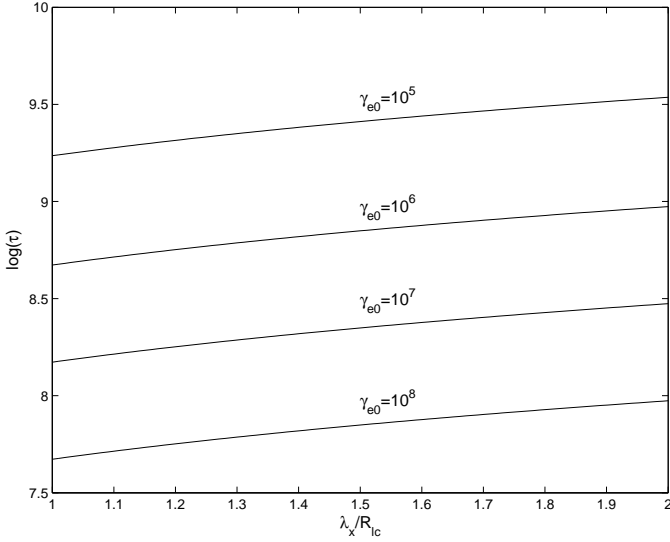


**Fig. 2.** The dependence of logarithm of the instability time scale on the normalized wave length. The set of parameters is:  $\gamma_{e0} = \{10^5; 10^6; 10^7; 10^8\}$ ,  $R_B \approx R_{lc}$ ,  $n_{e0} = 0.001 \text{ cm}^{-3}$ ,  $\lambda_\phi = 100R_{lc}$  and  $L/L_E = 0.01$ .

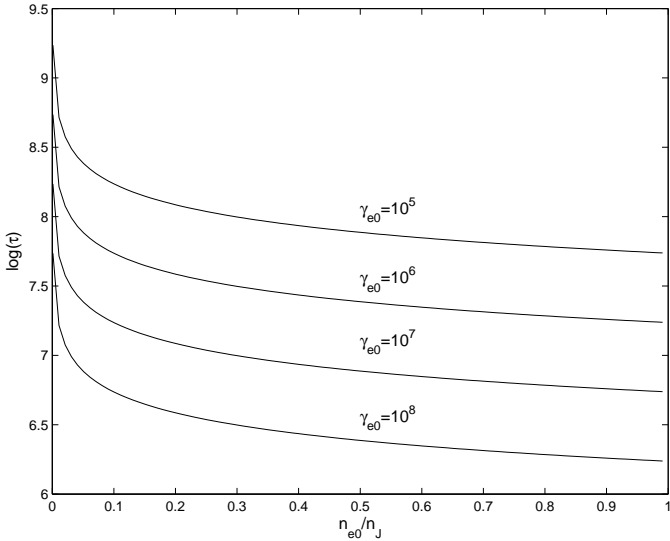


**Fig. 3.** The dependence of logarithm of the instability time scale on the density normalized by the medium density. The set of parameters is:  $\gamma_{e0} = \{10^5; 10^6; 10^7; 10^8\}$ ,  $R_B \approx R_{lc}$ ,  $\lambda_{e0} = R_{lc}$ ,  $\lambda_\phi = 100R_{lc}$  and  $L/L_E = 0.01$ .

### 3. Results

In this section we investigate the efficiency of the CDI for AGN winds. The behaviour of the growth rate will be studied versus the wave length, the density of relativistic electrons, their Lorentz factors and the AGN bolometric luminosity.

For studying the behaviour of the instability as a function of the wave length one can examine the typical AGN parameters:  $M_{BH} = 10^8 \times M_\odot$ ,  $\Omega = 5 \times 10^{-5} \text{ s}^{-1}$  and  $L = 10^{44} \text{ erg/s}$ , where  $M_{BH}$  is the AGN mass,  $M_\odot$  - solar mass and  $L$  is the bolometric luminosity of the AGN.

Let us consider Eq. (23) and plot logarithm of the instability time scale

$$\tau \equiv \frac{1}{\Gamma} \quad (24)$$

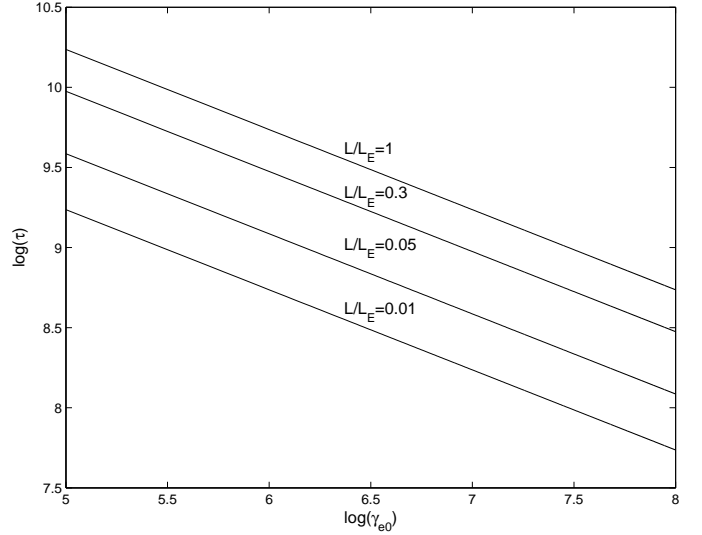


**Fig. 4.** The dependence of logarithm of the instability time scale on  $\log(\gamma_{e0})$ . The set of parameters is:  $R_B \approx R_{lc}$ ,  $n_{e0}/n_m = 0.001$ ,  $\lambda_{e0} = R_{lc}$ ,  $\lambda_\phi = 100R_{lc}$  and  $L/L_E = \{0.01; 0.05; 0.3; 1\}$ .

versus the wave length normalized by the light cylinder radius. The present consideration is based on the centrifugal acceleration. As it has been shown in (Osmanov et al. 2007), due to the CF, the relativistic particles may reach very high Lorentz factors. For this purpose it is reasonable to investigate the efficiency of the instability versus the wave length but for different values of Lorentz factors. Fig. 2 shows the mentioned behaviour for the following parameters:  $\gamma_{e0} = \{10^5; 10^6; 10^7; 10^8\}$ ,  $R_B \approx R_{lc}$ ,  $n_{e0} = 0.001 \text{ cm}^{-3}$ ,  $\lambda_\phi \equiv 2\pi/k_\phi = 100R_{lc}$  and  $L/L_E = 0.01$ , where  $L_E = 10^{46} \text{ erg/s}$  is the Eddington luminosity for the given AGN mass. Different curves correspond to different values of Lorentz factors. As it is clear from the plots, the time scale is a continuously increasing function of  $\lambda_x (\equiv 2\pi/k_x)$ , which is a direct consequence of Eqs. (22,23). Indeed, as we see from Eq. (22),  $\Xi_{0,\pm 1} \sim 1/\lambda_x$ , which combining with Eq. (23) gives  $\Gamma \sim 1/\sqrt{\lambda_x}$ . Therefore the bigger the initial perturbation wave length, the less the instability time scale and consequently the less the CDI efficiency. For the given range of  $\lambda_x$  and different values of  $\gamma_{e0}$ , the CDI time scale varies from  $\sim 10^7 \text{ s}$  ( $\lambda_x/R_{lc} = 1$ ,  $\gamma_{e0} = 10^8$ ) to  $\sim 10^9$  ( $\lambda_x/R_{lc} = 2$ ,  $\gamma_{e0} = 10^5$ ).

Since the CDI growth rate depends on the plasma frequency [see Eq. (23,22)], which in turn is the function of the density, it is obvious that the instability time scale must be influenced by the density of relativistic electrons in the AGN winds. Indeed, in Fig. 3 the plots of  $\log(\tau)$  versus the AGN wind density are shown and one can see that the time scale is the continuously decreasing function of  $n_{e0}/n_m$ . The set of parameters is the same as in Fig. 2, except  $\lambda_x = R_{lc}$  and  $n_{e0}/n_m \in \{0.001, 1\}$ . Here  $n_{e0}$  is normalized by the intergalactic medium density,  $n_m \approx 1 \text{ cm}^{-3}$ . As we see from the figure,  $\tau$  varies from  $\sim 10^9 \text{ s}$  ( $n_{e0}/n_m = 0.001$ ,  $\gamma_{e0} = 10^5$ ) to  $\sim 10^6 \text{ s}$  ( $n_{e0}/n_m = 1$ ,  $\gamma_{e0} = 10^8$ ).

In Fig. 4 the plot of  $\log(\tau)$  versus  $\log(\gamma_{e0})$  is shown for different luminosities. The set of parameters is the same as in Fig. 2 except the continuous range of  $\gamma_{e0} \in \{10^5; 10^8\}$ , different values of the luminosity  $L/L_E = \{0.01; 0.05; 0.3; 1\}$  and  $\lambda_x = R_{lc}$ . The figure shows the continuously decreasing behaviour of the instability time scale, which is a natural consequence of the fact that the more energetic electrons will induce the curvature drift instability more efficiently. Indeed, from Eq. (12) it is clear that the drift velocity is proportional to the Lorentz factor of the particle,

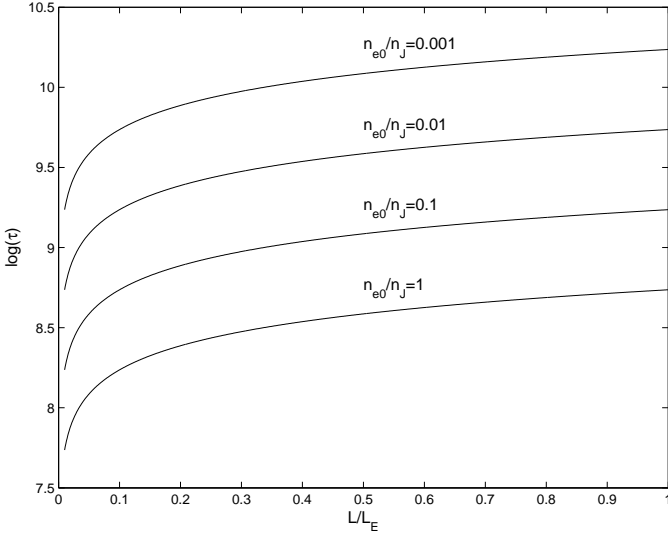


**Fig. 5.** The dependence of logarithm of the instability time scale on  $\log(\gamma_{e0})$ . The set of parameters is:  $R_B \approx R_{lc}$ ,  $n_{e0}/n_m = \{0.001; 0.01; 0.1; 1\}$ ,  $\lambda_{e0} = R_{lc}$ ,  $\lambda_\phi = 100R_{lc}$  and  $L/L_E = 0.01$ .

and hence the corresponding instability will be more efficient, leading to the decreasing behaviour of  $\log(\tau)$ . As we see the instability time scale varies from  $\sim 10^{10}s$  ( $\gamma_{e0} = 10^5$ ,  $L/L_E = 1$ ) to  $\sim 10^8s$  ( $\gamma_{e0} = 10^7$ ,  $L/L_E = 0.01$ ). On the other hand the plots for different luminosities exhibit another feature of the behaviour of  $\tau$ : by increasing the luminosity of the AGN, the corresponding instability becomes less efficient.

To see this particular feature more clearly, let us look at Fig. 5 exhibiting the dependence of  $\log(\tau)$  on  $L/L_E$  for different values of densities. From the plots it is seen that by increasing the luminosity, the time scale continuously increases. This behaviour follows from the fact, that the bigger the luminosity, the bigger the magnetic field [see Eq. (13)] and hence the less the drift velocity, leading to the less efficient CDI shown in the figure. By considering bigger values of densities, the CDI becomes more efficient, which we have already explained while considering Fig. 3. For the mentioned area of quantities (see Fig. 5), the time scale varies from  $\sim 10^7s$  ( $L/L_E = 0.01$ ,  $n_{e0}/n_J = 1$ ) to  $\sim 10^{10}s$  ( $L/L_E = 1$ ,  $n_{e0}/n_J = 0.001$ ).

We see from the present investigation that the instability time scale varies in the following range:  $\tau \in \{10^6; 10^{10}\}s$ . In order to specify how efficient is the CDI it is sensible to examine an accretion process, estimating the corresponding evolution time scale, and compare it with that of the CDI.

Considering the problem of fuelling of AGNs, in (King & Pringle 2007) it has been shown that the self gravitating mass in accretion flows can be estimated by the following expression:

$$M_{sg} = 2.76 \times 10^5 \left(\frac{\eta}{0.03}\right)^{-2/27} \left(\frac{\epsilon}{0.1}\right)^{-5/27} \left(\frac{L}{0.1L_E}\right)^{5/27} \times \left(\frac{M_{BH}}{10^8 M_\odot}\right)^{23/27} M_\odot, \quad (25)$$

where  $\eta$  and  $\epsilon$  are Shakura, Sunyaev viscosity parameter (Shakura & Sunyaev 1973) and the accretion parameter respec-

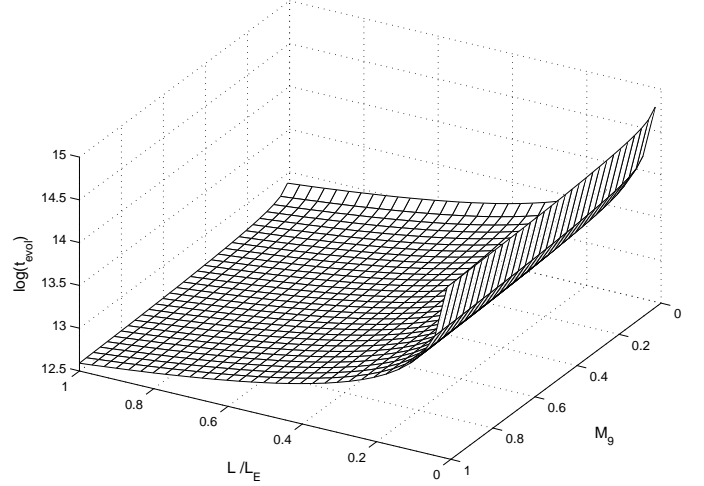


**Fig. 6.** The behaviour of logarithm of the evolution time scale versus  $M_9$  and  $L/L_E$ . The set of parameters is:  $\eta = 0.03$ ,  $\epsilon = 0.1$ .

tively. The latter can be defined by means of the accretion mass rate  $\dot{M}$  and the luminosity:

$$\epsilon \equiv \frac{L}{\dot{M}c^2}. \quad (26)$$

Then, defining the accretion time scale  $t_{evol} \equiv M_{sg}/\dot{M}$  one can reduce it to (King & Pringle 2007):

$$t_{evol} = 3.53 \times 10^{13} \left(\frac{\eta}{0.03}\right)^{-2/27} \left(\frac{\epsilon}{0.1}\right)^{22/27} \left(\frac{L}{0.1L_E}\right)^{-22/27} \times \left(\frac{M_{BH}}{10^8 M_\odot}\right)^{-4/27} s. \quad (27)$$

As it is clear from Eq. (27), the accretion evolution time scale depends on two major AGN parameters: on the luminosity ( $L$ ) and the AGN mass ( $M_{BH}$ ). Bearing in mind Eq. (27) it is sensible to investigate  $t_{evol}$  versus  $L$  and  $M_{BH}$ . For this purpose let us consider the possible maximum "area" of the parametric space,  $L - M_{BH}$  studying the behaviour of  $t_{evol}$  for the typical accretion disk parameters  $\eta = 0.03$ ,  $\epsilon = 0.1$ .

In Fig. 6 we show the two dimensional surface of logarithm of the evolution time scale. The variables are in the following range:  $M_9 \equiv M_{BH}/(10^9 \times M_\odot) \in \{0.01; 1\}$  and  $L/L_E \in \{0.01; 1\}$ . For plotting the figure we took into account that according to the observations AGN masses vary in the following range:  $M_{BH} \in \{10^6; 10^9\} \times M_\odot$  (Nelson 2000). As it is clear from Fig. 6,  $t_{evol}$  is a continuously decreasing function of  $M_9$  and  $L/L_E$ . The minimum value of the evolution time scale ( $\sim 10^{12}s$ ), when the accretion process is extremely efficient corresponds to  $M_9 = 1$  and  $L/L_E = 1$ , whereas the maximum value being of the order  $\sim 10^{15}s$  corresponds to the following pair of the variables:  $M_9 = 0.001$  and  $L/L_E = 0.01$ .

For understanding how efficient is the curvature drift instability, one has to compare the corresponding time scale with the evolution time scale. As it has been found, depending on physically reasonable parameters  $\tau$  varies in the range:  $\sim 10^6-10^8s$ , whereas the sensible area of  $t_{evol}$  is:  $\sim 10^{12-15}s$ . Therefore the instability time scale is less than the evolution time scale of the

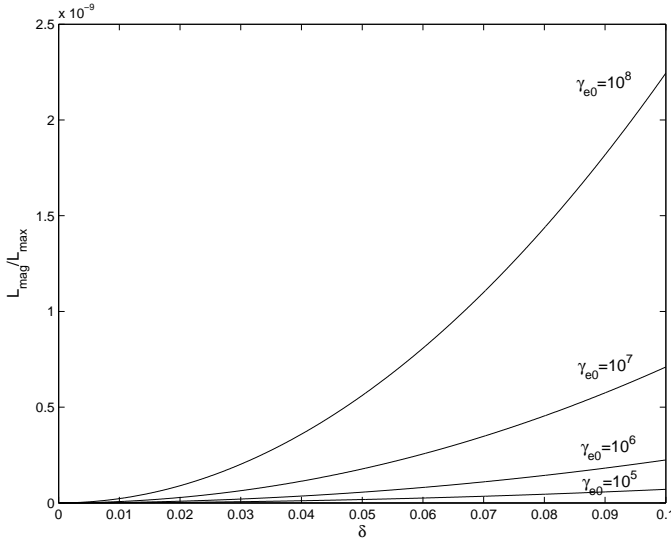


**Fig. 7.** The dependence of  $L_m/L_{max}$  versus  $\delta$ . The set of parameters is:  $\gamma_{e0} = \{10^5; 10^6; 10^7; 10^8\}$ ,  $R_B \approx R_{lc}$ ,  $n_{e0} = 0.001 cm^{-3}$ ,  $\lambda_\phi = 100R_{lc}$ ,  $\lambda_x = R_{lc}$  and  $L = 10^{45} erg/s$ .

accretion by many orders of magnitude, which means that the linear stage of the CDI is extremely efficient.

The twisting process of magnetic field lines requires a certain amount of energy and it is natural to study also the energy budget of this process. For this reason one has to introduce the maximum of the possible luminosity  $L_{max} = \dot{M}c^2$  and compare it with the "luminosity" corresponding to the reconstruction of the magnetic field configuration  $L_m \equiv \Delta E_m / \Delta t \approx \Delta E_m / \tau$ . (here  $\Delta E_m$  is the variation of the magnetic energy due to the curvature drift instability).

Let us consider the AGN with the luminosity,  $L = 10^{45} erg/s$ , then by applying Eq. (26) and taking into account  $\epsilon = 0.1$  one can show that the accretion may provide the following maximum value:

$$L_{max} = 10^{46} erg/s. \quad (28)$$

On the other hand if the process of sweepback is realistic, the magnetic "luminosity" can not exceed  $L_{max}$ . Since this process takes place in the nearby zone of the LCS, the effective spatial volume can be estimated by the following expression:

$$\Delta V \approx R_{lc}^2 \Delta R = R_{lc}^3 \kappa, \quad (29)$$

where  $\kappa \equiv \Delta R / R_{lc} \ll 1$  represents the non dimensional thickness of the considered spatial zone. Taking into account Eq. (29) the expression of the magnetic "luminosity" reduces to:

$$L_m = \frac{B_r^2}{4\pi\tau} R_{lc}^3 \kappa, \quad (30)$$

where  $B_r$  due to the CDI behaves in time as:

$$B_r = B_r^0 e^{t/\tau} \quad (31)$$

Here  $B_r^0$  is the initial perturbation of magnetic field's toroidal component.

Let us introduce the initial non dimensional perturbation,  $\delta$ , defined as:  $\delta \equiv B_r^0 / B_0$ , where by  $B_0$  we denote the induction of the magnetic field in the leading state [see Eq. (31)]. By considering the following set of parameters:  $\gamma_{e0} = \{10^5; 10^6; 10^7; 10^8\}$ ,

$R_B \approx R_{lc}$ ,  $n_{e0} = 0.001 cm^{-3}$ ,  $\lambda_\phi = 100R_{lc}$ ,  $\lambda_x = R_{lc}$  and  $L = 10^{45} erg/s$ , one can plot the behaviour of  $L_m/L_{max}$  versus the initial perturbation for the characteristic time scale ( $t \approx \tau$ ). As we see from Fig. 7,  $L_m/L_{max}$  varies from  $\sim 0$  ( $\delta = 0$ ) to  $\sim 2.3 \times 10^{-9}$  ( $\delta = 0.1$ ,  $\gamma_{e0} = 10^8$ ). Therefore the maximum luminosity (thus the total luminosity budget) exceeds by many orders of magnitude the magnetic "luminosity" required for the twisting of the field lines. This means that only a tiny fraction of the total energy goes to the sweepback, making this process feasible.

## 4. Summary

1. Considering the relativistic two component plasma for AGN winds the centrifugally driven curvature drift instability has been studied.
2. Taking into account a quasi single approach for the particle dynamics, we linearized the Euler, continuity and induction equations. The dispersion relation characterizing the parametric instability of the toroidal component of the magnetic field has been derived.
3. Considering the proper frequency of the curvature drift modes, the corresponding expression of the instability increment has been obtained for the light cylinder region.
4. Efficiency of the CDI has been investigated by adopting four physical parameters, namely: the wave length, the flow density and the Lorentz factors of electrons and the luminosity of AGNs.
5. By considering the evolution process of the accretion, the corresponding time scale has been estimated for a physically reasonable area in the parametric space  $L - M_{BH}$ . It was shown that the instability time scale was less by many orders of magnitude than the evolution time scale, indicating extremely high efficiency of the CDI.
6. Examining the instability from the point of view of the energy budget, we have seen that the sweepback of the magnetic field lines requires only a small fraction of the total energy, which means that the CDI is a realistic process.

An important restriction of the present work is that for describing the plasma kinematics a single particle approach has been applied. On the other hand it is natural to suppose that the collective phenomena must strongly influence the overall kinematic picture of the plasma motion. For understanding how the mentioned fact changes the instability, one has to generalize the present model for a more realistic astrophysical scenario.

The next limitation is related to the fact that the magnetic field lines were supposed to be quasi rectilinear, whereas in real astrophysical situations the field lines might be initially curved. This particular case also needs to be studied generalizing the present model.

In this paper the field lines located in the equatorial plane have been considered, although in realistic situations the magnetic field lines also might be inclined with respect to the equatorial plane. Therefore it is essential to examine this particular case as well and see how the efficiency of the CDI changes, when the mentioned inclination angle is taken into account.

*Acknowledgements.* I thank professor G. Machabeli for valuable discussions. The research was supported by the Georgian National Science Foundation grant GNSF/ST06/4-096.

## References

Blandford R.D., 2002, *lum. conf.*, 381B

- Blandford, R. D., & Payne, D. G., 1982, MNRAS, 199, 883
- Chedia O.V., Kahniashvili T.A., Machabeli G.Z. & Nanobashvili I.S., 1996, Astrophys. Space Sci. 239, 57.
- Gangadhara R.T., Lesch H. 1997, A&A, 323, L45
- King A. R. & Pringle J. E., 2007, MNRAS, 377, 25
- Machabeli G., Osmanov Z. & Mahajan S., 2005, Phys. Plasmas 12, 062901
- Machabeli G. & Rogava A. D., 1994, Phys.Rev. A, 50, 98
- Nelson, Charles H., 2000, ApJ, 544L, 91N
- Osmanov Z., 2008, Phys. Plasmas, 15, 032901
- Osmanov Z., Dalakishvili Z. & Machabeli Z. 2008a, MNRAS, 383, 1007
- Osmanov Z., Shapakdze D. & Machabeli G., 2008b, ApJ, (submitted)
- Osmanov Z., Rogava A.S. & Bodo G., 2007, A&A, 470, 395
- Rieger F. M. & Aharonian F. A., 2008, A&A, 479, 5
- Rogava A. D., Dalakishvili G. & Osmanov Z., 2003, Gen. Rel. and Grav. 35, 1133
- Shakura N. I. & Sunyaev R. A., 1973, A&A, 24, 337
- Silin V.P. & Tikhonchuk V.T., 1970, J. Appl. Mech. Tech. Phys., **11**, 922
- Spitkovsky A., 2004, 'Young Neutron Stars and Their Environments, IAU Symposium no. 218, held as part of the IAU General Assembly, 14-17 July, 2003 in Sydney, Australia. Edited by Fernando Camilo and Bryan M. Gaensler. San Francisco, CA: Astronomical Society of the Pacific, 2004, p.357
- Spitkovsky A. & Arons J., 2002, ASP Conf. Ser., 271, 81S